Journal of Photochemistry and Photobiology A: Chemistry 221 (2011) 113–122

Contents lists available at ScienceDirect

Journal of Photochemistry and Photobiology A: Chemistry

journal homepage: www.elsevier.com/locate/jphotochem

Photoinduced transmembrane electron transport in DPPC vesicles: Mechanism and application to a hydrogen generation system

Kentaro Watanabe, Kimio Moriya, Tetsu Kouyama, Ayumi Onoda, Tomiaki Minatani, Shin-ya Takizawa, Shigeru Murata*

Department of Basic Science, Graduate School of Arts and Sciences, The University of Tokyo, Meguro-ku, Tokyo 153-8902, Japan

ARTICLE INFO

Article history:
Received 28 December 2010
Received in revised form 1 April 2011
Accepted 22 April 2011
Available online 30 April 2011

Keywords:
Electron transport
Vesicle
Pyrene
Fluorescence
Hydrogen generation

ABSTRACT

Pyrene-sensitized transmembrane electron transport from ascorbate (Asc^-) in the inner waterpool to methylviologen (MV^{2+}) in the outer aqueous solution proceeded in gel-phase DPPC vesicles, in which the lateral diffusion of molecules embedded in the vesicle bilayers is totally restricted. Based on the effects of the sensitizer concentration and cholesterol added to DPPC membranes on the efficiency of the electron transport, we propose that the sensitizer clusters play an essential role in the electron transport in DPPC vesicles. The presence of the sensitizer clusters in DPPC vesicles is supported by the temperature dependence of the intensity ratio of the excimer to the monomer fluorescence of the sensitizer. We found that this photoinduced transmembrane electron transport system works using various electron donors that undergo a reversible redox cycle other than Asc^-, and that there is a tendency for electron donors having lower oxidation potential to give a larger rate of $MV^{+\bullet}$ formation. Moreover, we accomplished the connection of the system of the photoinduced transmembrane electron transport in DPPC vesicles with the system for hydrogen generation from water using colloidal platinum as a catalyst.

1. Introduction

Photochemical processes in structurally ordered multimolecular systems are of great interest in view of the development of technologies for photoactive molecular devices and the construction of artificial molecular systems for solar energy conversion [1–6]. In natural photosynthesis in green plants, in which solar energy is converted into chemical potential with high efficiency and stored in carbohydrates, the phospholipids bilayer membrane plays an essential role [7,8]. The membrane supports the reaction centers in which the molecules that participate in light absorption and charge separation are spatially organized so that vectorial electron transfer across the membrane is achieved. Moreover, the membrane maintains the difference in chemical potential generated photochemically between two aqueous phases, which is utilized as the driving force of redox reactions and ATP production. Thus, the most primitive aspect of photosynthesis is a photoinduced transmembrane electron transport to generate a long-lived charge separated state.

Studies of photoinduced transmembrane electron transport mimicking natural photosynthetic systems started in the 1970s using vesicles as reaction fields [9,10]. Vesicles are spherical, multimolecular aggregates formed by self-organization of amphiphiles, in which a hydrophobic membrane separates an inner waterpool from the bulk aqueous phase [11,12]. Calvin and his co-workers reported that endoergic electron transport from EDTA entrapped in the inner waterpool of vesicles to methylviologen (*N*,*N*′-dimethyl-4,4′-bipyridinium, MV^{2+}) dissolved in the outer aqueous solution could be driven by the irradiation of the tris(bipyridine)ruthenium derivative embedded in the bilayer membrane [10]. This pioneering work demonstrated that electron transport through a hydrophobic membrane could be carried out without any membrane components acting as electron carriers. The authors proposed that the transmembrane electron transport occurred by a mechanism involving electron exchange between the sensitizers located in opposing monolayers of the vesicles [13].

A number of systems of photoinduced electron transport across vesicle bilayers have been reported, which indicates the usefulness of vesicles for mimicking natural photosynthetic systems [14,15]. In almost all cases, however, sacrificial electron donors such as ethylenediaminetetraacetic acid (EDTA) and triethanolamine (TEOA) are used to suppress the recombination of photogenerated charges. As these molecules decompose irreversibly after donating electrons, photoinduced transmembrane electron transport systems using sacrificial electron donors are of no significance from the viewpoint of light energy conversion and its storage. Recently, we reported that pyrene derivatives embedded into the vesicle bilayers of phosphatidylcholine (PC) from egg yolks

* Corresponding author. Tel.: +81 3 5454 6596; fax: +81 3 5454 6998.
E-mail address: cmura@mail.ecc.u-tokyo.ac.jp (S. Murata).

1010-6030/$ – see front matter © 2011 Elsevier B.V. All rights reserved.
doi:10.1016/j.jphotochem.2011.04.034

induced photochemically electron transport from ascorbate (Asc^-) entrapped into the inner waterpool to MV^{2+} dissolved in the outer aqueous solutions [16–18]. Asc^- undergoes a reversible redox reaction with semidehydroascorbate ($Asc^{\bullet}$), which disproportionates to give dehydroascorbate and Asc^- [19]. The free-energy change for the electron transfer from Asc^- to MV^{2+} is estimated to be +12.7 kcal mol^{-1} [20]. Thus, although our system cannot work using visible light, we believe that it is one of the most faithful models of natural photosynthesis in that an electron is transferred from the inside to the outside of closed bilayers membranes with the aid of light energy between two reversible redox couples in the energetically uphill direction.

A number of factors are considered to affect the efficiency of pyrene-sensitized electron transport across vesicle bilayers. We demonstrated that the efficiency of the electron transport is sensitive to the substituent group of the pyrenyl ring; a hydrophilic functional group linked with the pyrene nucleus by a short methylene chain is necessary to act as an excellent sensitizer [17]. It is thought that electron transport efficiency is also controlled by the structure of PC molecules employed in the vesicle formation, which affects the physical properties of vesicle membranes. In particular, the molecular dynamics and the structural organization of vesicle membranes are considerably different between temperature ranges above and below the phase transition temperature, T_m, which is controlled by the length of hydrophobic alkyl chains of PC molecules, as well as whether the alkyl chains of PC molecules are saturated or unsaturated [21]. Above T_m, vesicle membranes are in a liquid-crystalline phase where lipid molecules can diffuse laterally with the diffusion coefficient, D_{diff}, of $\sim 10^{-8}$ cm^{-1} s^{-1}, whereas when the temperature is lowered below T_m, transition to the gel phase occurs, in which the lateral diffusion of lipid molecules is almost frozen [22,23]. In order to reveal the effect of the physical properties of vesicle membranes on the efficiency of pyrene-sensitized transmembrane electron transport, we investigated the reaction using vesicles composed of 1,2-dipalmitoyl-*sn*-glycero-3-phosphocholine (DPPC) in the reaction field. DPPC vesicles are in the gel phase at room temperature, T_m of which is 42 °C, in contrast to the liquid-crystalline vesicles of PC from egg yolks (T_m < 0 °C) that were employed in our previous work. It is expected that if the diffusion of sensitizers embedded in the vesicle bilayers participates in the transmembrane electron transfer process, the total efficiency of the photoinduced electron transport across vesicle bilayers would be reduced considerably in DPPC vesicles in which the diffusion of molecules are totally restricted. We found, however, that photoinduced transmembrane electron transport proceeded in DPPC vesicles with an efficiency comparable to that in the liquid-crystalline vesicles composed of 1-palmitoyl-2-oleoyl-*sn*-glycero-3-phosphocholine (POPC, T_m = −3 °C). In this paper, we present detailed data on pyrene-sensitized transmembrane electron transport in DPPC vesicles, and discuss the mechanism on the basis of the photophysical behaviors of sensitizers in the vesicles. Moreover, attempts to apply our transmembrane electron transport system to the photochemical hydrogen production using colloidal platinum particles are also reported.

2. Experimental

2.1. General methods

UV–vis spectra were recorded on a JASCO V-560 spectrometer. Fluorescence spectra were recorded on a JASCO FP-777 spectrofluorometer with a 200 nm min^{-1} scanning speed and a 1.5 nm bandwidth on excitation at 350 nm. The sample temperature in fluorescence measurement was regulated by using a JASCO ECT-271 Peltier cell holder. 1-(Hydroxymethyl) pyrene ($PyCH_2OH$) was purchased from Aldrich, and cholesterol was purchased from Wako and used after recrystallization. 1,2-Dipalmitoyl-*sn*-glycero-3-phosphocholine (DPPC), 1-palmitoyl-2-oleoyl-*sn*-glycero-3-phosphocholine (POPC), *N*,*N*′-dimethyl-4,4′-bipyridinium dichloride trihydrate ($MVCl_2{\cdot}3H_2O$), L-cysteine (CySH), and L-glutathione (GSH) were purchased from Sigma–Aldrich, sodium ascorbate (AscNa), triethanolamine (TEOA) and tris(hydroxymethyl)aminomethane (Tris) were purchased from Tokyo Kasei Kogyo Co., Ltd., and ethylenediaminetetraacetic acid disodium salt (EDTA 2Na) was purchased from Wako and used without purification.

2.2. Vesicle preparation

A $CHCl_3$ solution of $PyCH_2OH$ (0.52 μmol) and DPPC (12.0 μmol) was evaporated under reduced pressure to form a thin film in a flask. The film was dried under vacuum overnight, and dispersed in a solution (4 mL) of 1.0 M tris(hydroxymethyl)aminomethane–HCl (Tris–HCl) buffer, pH 7.5, containing 1.0 M AscNa by vortex mixing (Sibata, TTM-1). The resulting suspension was treated with ultrasonic process (Iwaki, USC-100Z38S-22) for 2 h at 55–60 °C. The solution was developed on a column with Sephadex G-50 (Amersham Biosciences) equilibrated with a 1.0 M Tris–HCl buffer solution containing 1.0 M NaCl to remove the sensitizer and AscNa outside the vesicles, and the fraction containing the amphiphile was collected to give the vesicle solution (11.4 mL). A solution of POPC vesicles was prepared in the same manner as that described above, except that the ultrasonic process was done under Ar at 20–30 °C. To the solution (3.0 mL) was added $MVCl_2{\cdot}3H_2O$ (30 mmol) to give a vesicle solution for electron transport experiments. The concentration of $PyCH_2OH$ in the vesicle solution, C_s, was evaluated by the absorbance at the wavelength of its maximal absorption and its molar extinction coefficient determined in $CHCl_3$; 345 nm (ε = 35,600 M^{-1} cm^{-1}). Dynamic light scattering studies of vesicle solutions were made on a Honeywell Microtac UPA-150 at room temperature.

2.3. Photochemistry

A vesicle solution was placed into a quartz cell (10 mm × 10 mm), and Ar was bubbled into the solution for 1 h. The solution was irradiated with a 500 W xenon arc lamp through both an optical cutoff filter (UV-35, >350 nm) and a band pass filter (UV-D36B, 360 ± 20 nm). The light intensity at the cell position was measured by the use of a photon counting meter (Ushio, UIT-150) and adjusted to 1.00 mW cm^{-2} at 365 nm. The $MV^{+\bullet}$ accumulation was monitored by an increase in the absorption of 604 nm, and the concentration of $MV^{+\bullet}$, [$MV^{+\bullet}$], was calculated by using its molar extinction coefficient (ε = 12,400 M^{-1} cm^{-1}) [10,24].

2.4. Fluorescence quenching studies

A solution of DPPC–cholesterol vesicles for fluorescence quenching studies was prepared in the same manner as that described above, and placed in a quartz cell (10 mm × 10 mm). To the solution was added a solution of $MVCl_2{\cdot}3H_2O$ in 1.0 M Tris–HCl buffer containing 1.0 M NaCl. Fluorescence spectra were measured at room temperature under air on excitation at 350 nm. Relative fluorescence intensities, I_0/I, were determined by measuring the peak of heights for the maxima. Quenching of the $PyCH_2OH$ fluorescence by various electron donors was studied in a 1.0 M Tris–HCl buffer solution containing 1.0 M NaCl. The fluorescence lifetime was measured by using a pulsed Q-switch Nd:YAG laser (SOLAR LF114) as the excitation source. The fluorescence decay profiles

were recorded by the use of third harmonic generation of the laser that provided UV pulses at 355 nm with duration of 13 ns.

2.5. Hydrogen generation

A vesicle solution for hydrogen generation experiments was prepared in the same manner as that described above, except that the concentrations of Tris–HCl, NaCl, and AscNa in the solution were 0.20 M. An aqueous solution containing PVP-protected platinum particles was prepared by irradiation of platinum metal plate in an aqueous solution (10 mL) of PVP (30 mg) with a Nd:YAG laser (Quanta-ray GCR-170, 1064 nm) according to the procedure of Mafuné and Kondow [25]. The concentration of platinum was adjusted to 1 mM by monitoring the weight loss of the metal plate after the laser ablation. The amounts of hydrogen evolved were determined by gas chromatography (J-Science Lab. Co., Ltd., GC7000TF) with a thermal conductivity detector and an activated carbon column (3 m × 3 mm).

3. Results and discussion

3.1. Pyrene-sensitized reduction of MV^{2+} with Asc^- incorporated into DPPC vesicles

In all experiments described in this paper, 1-(hydroxymethyl)pyrene $PyCH_2OH$, a pyrene having high ability to sensitize electron transport across vesicle bilayers of egg yolks PC [16,17], was employed as a sensitizer. Vesicle solutions used for the electron transport experiments were prepared as described in Section 2. By the use of a dynamic light scattering method, it was confirmed that the solution contained particles with a diameter of 30–80 nm indicating the formation of vesicles having a unilamellar structure (Fig. S1). In the UV absorption spectrum of the vesicle solution, intense transitions with maxima at 345, 329, and 315 nm appeared, which demonstrates the incorporation of $PyCH_2OH$ into the vesicles. The concentration of the sensitizer in the vesicle solution, C_s, was evaluated to be 27.7 μM by using its molar extinction coefficient determined in $CHCl_3$, indicating that 61% of the sensitizer molecules employed in the vesicle preparation were incorporated into the vesicles and that the fraction of the sensitizer in the vesicles was 2.5 mol% by assuming that all DPPC molecules employed in the vesicle preparation were present in the vesicle solution. The incorporation of the sensitizer into the vesicle solution was also monitored by the fluorescence spectrum, which showed the characteristic signals of pyrene derivatives having maxima at 378 and 398 nm, together with an intense and broad peak at 480 nm that was assigned to the excimer emission [26,27].

The absorption and fluorescence spectra of $PyCH_2OH$ recorded in the vesicle solution before the addition of MV^{2+} are shown in Fig. 1, together with those in the vesicle solution prepared in an identical manner except for using POPC instead of DPPC. The maximal wavelengths of the absorption and fluorescence spectra were identical in both vesicle solutions, although the concentration of the sensitizer molecules incorporated into the POPC vesicles (C_s = 32.2 μM) was slightly higher compared with that in DPPC vesicles. However, it should be emphasized that the relative intensity of the excimer fluorescence in the POPC vesicles was considerably smaller than that in DPPC vesicles. When the excimer to monomer fluorescence intensity ratio, I_e/I_m, is defined as a ratio of the intensity at 480 nm to that at 398 nm in the fluorescence spectrum, the I_e/I_m values are determined to be 0.777 in the DPPC vesicles and 0.251 in the POPC vesicles. The I_e/I_m value of parent pyrene or pyrene derivatives embedded in PC vesicles is sensitive to their lateral mobility and distribution [28–32]. On the basis of the concentration and temperature dependences of the I_e/I_m values for

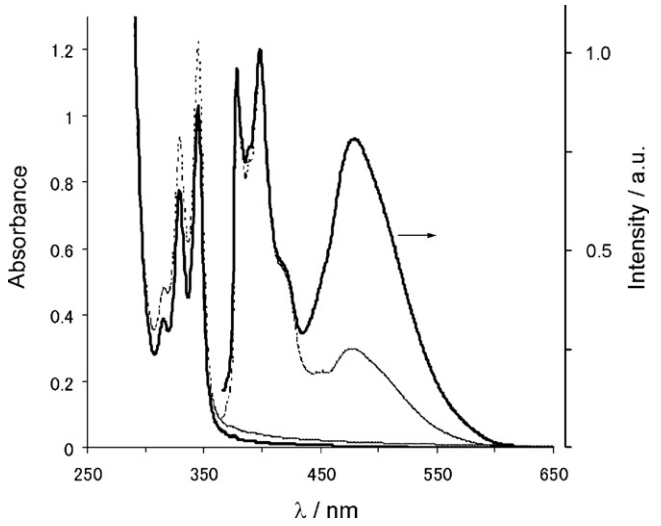

Fig. 1. Absorption and fluorescence (λ_{ex} = 350 nm) spectra of $PyCH_2OH$ recorded in DPPC (solid line) and POPC (broken line) vesicle solutions.

pyrene embedded in DPPC membranes, Galla and Sackmann determined the diffusion coefficient, D_{diff}, for pyrene and concluded that pyrene aggregates into small clusters below T_m [28–30]. The reason for the considerable difference in the I_e/I_m value between the DPPC and POPC vesicles, as well as its influence on the efficiency of the photoinduced transmembrane electron transport, is discussed in detail in the following section.

On the excitation of $PyCH_2OH$ in the DPPC vesicle solution containing Asc^- and MV^{2+} in the inner waterpool of the vesicle and in the outer aqueous phase, respectively, with a 500-W xenon arc lamp through optical glass filters (366 ± 15 nm), the reduction of MV^{2+} was observed to produce $MV^{+\bullet}$, which was identified by its characteristic absorption with maxima at 396 and 604 nm. In Fig. 2, the accumulation of $MV^{+\bullet}$ by the irradiation of a DPPC vesicle solution is demonstrated, together with that of a POPC vesicle solution prepared in an identical manner except for using POPC instead of DPPC.

In a previous paper, we proposed that the photoinduced reduction of MV^{2+} proceeds mainly by a mechanism involving the

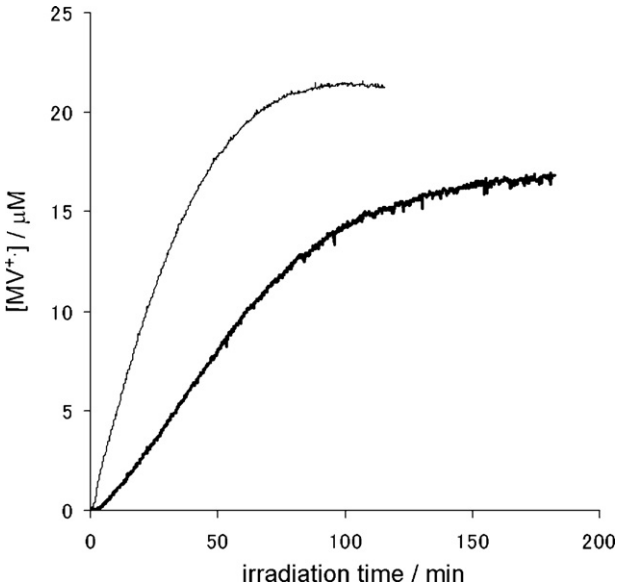

Fig. 2. Accumulation of $MV^{+\bullet}$ by the irradiation of a solution of DPPC (bold line) and POPC (thin line) vesicles containing $PyCH_2OH$ and Asc^-.

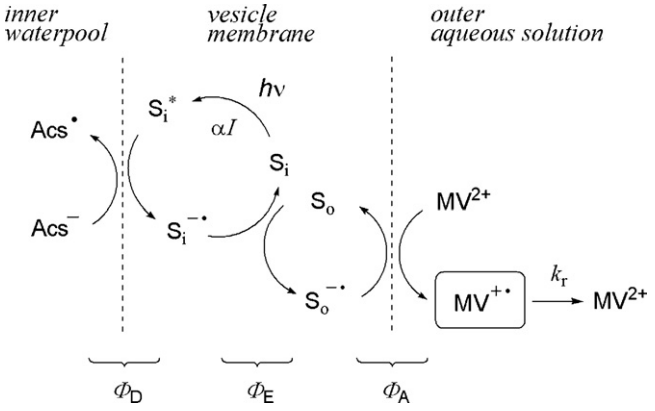

Scheme 1. Proposed mechanism for the formation of $MV^{+\bullet}$ initiated by the quenching of $PyCH_2OH$ in its singlet excited state (S_i^*) by Asc^- entrapped in the inner waterpool of DPPC vesicles [17,18].

reductive quenching of the singlet excited state of the sensitizer by Asc^- to produce a sensitizer radical anion, followed by electron exchange between the sensitizers located at the inner and outer interfaces across the vesicle membrane (Scheme 1) [17,18].

According to this scheme, the rate of $MV^{+\bullet}$ formation, v_i, is described by $aI\Phi_D\Phi_E\Phi_A$, where a is the proportion of sensitizers located at the interface of the vesicle bilayers and the inner waterpool, and I is the number of photons absorbed by the sensitizer in unit time. Moreover, Φ_D, Φ_E, and Φ_A represent the efficiency for quenching of the sensitizer excited state by Asc^-, the efficiency for the electron exchange between the sensitizers located at the inner and outer interfaces, and the efficiency for the electron transfer of the sensitizer radical anion to MV^{2+}, respectively. As shown in Fig. 2, in the photoinduced electron transport in POPC vesicles, an increase in the $MV^{+\bullet}$ concentration, $[MV^{+\bullet}]$, with irradiation time, t, obeyed good first-order kinetics, $[MV^{+\bullet}] = A_m[1 - \exp(-k_r t)]$. The observation indicates that upon irradiation the $MV^{+\bullet}$ formation proceeds at the steady rate of v_i, which can be evaluated as $A_m k_r$, where k_r is the pseudo-first-order rate constant for the $MV^{+\bullet}$ disappearance by the reaction with an electron-accepting species, such as the oxidized form of Asc^- escaping from the inner waterpool and contaminating molecular oxygen. On the other hand, on the irradiation of the DPPC vesicle solution, the concentration of $MV^{+\bullet}$ increased approximately linearly with the irradiation time after a short induction period and attained maximal concentration, C_{max}. Thus, the rate of $MV^{+\bullet}$ formation, v_i, in the DPPC vesicle solution was evaluated to be 0.178 μM min^{-1} from the linear portion of the $MV^{+\bullet}$ accumulation curve, which was smaller than 0.615 μM min^{-1} determined in the POPC vesicle solution. Moreover, the maximal concentration of photogenerated $MV^{+\bullet}$, C_{max}, which depends on not only the rate of $MV^{+\bullet}$ formation, v_i, but the rate constant for the $MV^{+\bullet}$ disappearance, k_r, was also lower in the DPPC vesicle solution than in the POPC vesicle solution; C_{max} = 16.8 μM and 21.6 μM in the DPPC and POPC vesicle solutions, respectively.

Thus, the photoinduced transmembrane electron transport proceeds in DPPC vesicles that are in the gel phase, analogously to the liquid-crystalline vesicles of egg yolks PC or POPC, although the values of v_i and C_{max} in the gel vesicles are slightly inferior to those in the liquid-crystalline vesicles prepared and irradiated under the same conditions.

3.2. Dependence on sensitizer concentration

As described in the previous section, the reduction of MV^{2+} dissolved in the outer aqueous phase by Asc^- entrapped in the inner waterpool of the DPPC vesicle solution occurs by the excitation of $PyCH_2OH$ embedded in the vesicle membrane. The concentration of the sensitizer in the DPPC membrane was 2.5 mol%, which implies that if the sensitizers are randomly distributed in the membrane, the average distance between two adjacent sensitizers is estimated to be 5.4 nm by assuming that the area per DPPC lipid molecule is 0.58 nm^2 [23]. Therefore, taking into account that the 'face to face' structure having an interfacial distance of ~0.35 nm is favored for pyrene excimer [27], the intense excimer emission observed in DPPC vesicles that are in the gel phase suggests that the sensitizers are not randomly distributed, but aggregate into small clusters in which the pyrene chromophores of the sensitizers are closely packed. Thus, in order to gain information about the aggregation of $PyCH_2OH$ embedded in DPPC vesicle bilayers and its influence on the efficiency of the photoinduced transmembrane electron transport, dependence of the excimer to monomer fluorescence intensity ratio, I_e/I_m, as well as the rate of $MV^{+\bullet}$ formation, v_i, on the sensitizer concentration was examined and compared with that obtained in the liquid-crystalline POPC vesicle bilayers.

3.2.1. Dependence of the rate of $MV^{+\bullet}$ formation, v_i

The concentration of $PyCH_2OH$ in the vesicle solution, C_s, could be controlled by the ratio of $PyCH_2OH$ to a constant DPPC amount (12 μmol) in the vesicle preparation. The electron transport experiments were carried out in the vesicle solutions of various C_s, and the rate of $MV^{+\bullet}$ formation, v_i, was determined. The dependence of v_i on C_s in the DPPC vesicle solution is depicted in Fig. 3a, together with that observed in the POPC vesicle solution. As shown in the figure, no large dependence of v_i on C_s was observed in the concentration ranges examined in both vesicle solutions. The number of photons absorbed by the sensitizer in unit time, I, increases with an increase in C_s. Since the light from a xenon arc lamp through optical filters (366 ± 15 nm) was employed in the irradiation, the relative value of I for each sensitizer concentration, I(rel), is estimated by the integration of $I_f(\lambda)(1 - 10^{-\varepsilon(\lambda)C_s l})$, where $I_f(\lambda)$ stands for the wavelength dependence of incident light evaluated by the spectrum of the light transmitted by the filters employed in the electron transport experiment, $\varepsilon(\lambda)$ shows the absorption spectrum of $PyCH_2OH$, and l is the length of the cell used in the irradiation experiment [17]. As mentioned in the previous section, v_i is depicted by $aI\Phi_D\Phi_E\Phi_A$, so that the relative value of the total efficiency of $MV^{+\bullet}$ formation, Φ_t(rel), is estimated by v_i/I(rel). Fig. 3b depicts the dependence of Φ_t(rel) on C_s in the DPPC and POPC vesicle solutions, indicating that the efficiency of photoinduced transmembrane electron transport decreases with an increase in the sensitizer concentration in both vesicle solutions. As shown in the figure, however, the dependence profile in the DPPC vesicle solution is significantly different from that in the POPC solution; the efficiency in the DPPC vesicle solution is almost unchanged in the C_s range above 10 μM, while the efficiency in the POPC vesicle solution decreases continuously with an increase in C_s. As discussed in detail in the following section, it seems that the difference in the dependence of Φ_t on C_s between the two vesicle solutions is derived from the difference in the phase of each vesicle membrane.

3.2.2. Dependence of the excimer to monomer fluorescence intensity ratio, I_e/I_m

As mentioned in the previous section, a broad emission with a maximum at 480 nm due to the excimer of $PyCH_2OH$ incorporated into the vesicle membrane was observed in the fluorescence spectra of the vesicle solution. We found the excimer to monomer fluorescence intensity ratio, I_e/I_m, was very sensitive to the concentration of $PyCH_2OH$ in the vesicle solution, C_s. It is generally accepted that the excimer formation is described by Scheme 2 [26–31], where M^* and $(MM)^*$ are excited monomer and excimer molecules, k_{fm} and k_{fe} are the transition probabilities for the radiative decay of M^* and $(MM)^*$, and k_{dm} and k_{de} are the transition probabilities for nonradiative decay of M^* and $(MM)^*$, respectively. Moreover, k_a is the

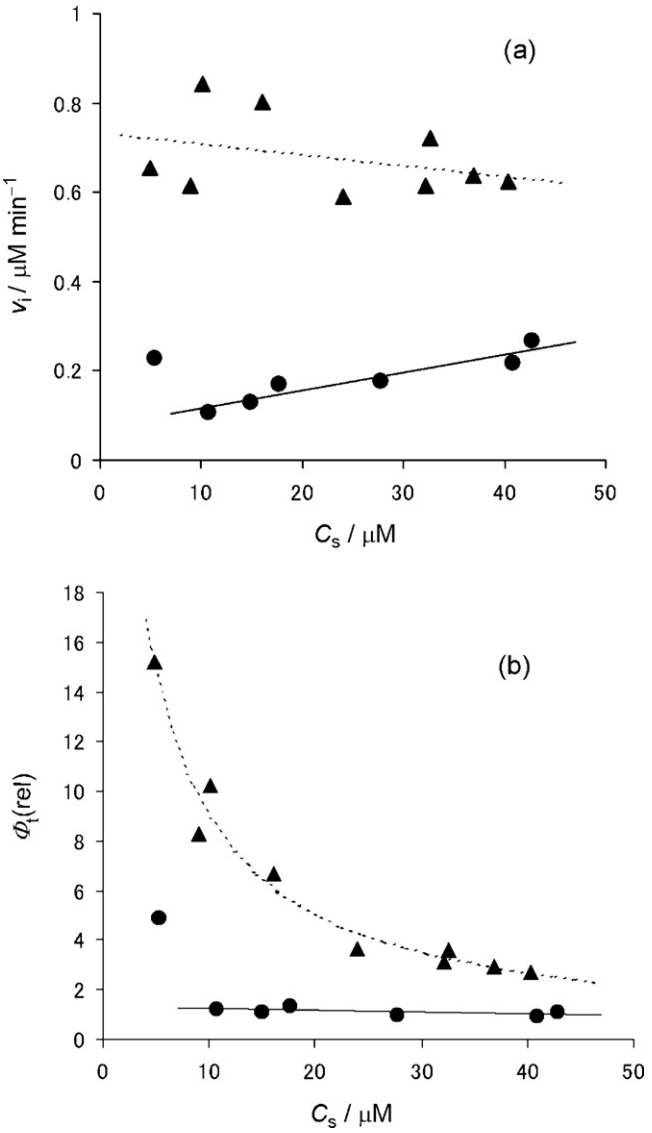

Fig. 3. Dependence of (a) the rate of $MV^{+\bullet}$ formation, v_i, and (b) the relative value of the total efficiency of $MV^{+\bullet}$ formation, Φ_t(rel), on the concentration of $PyCH_2OH$ in the DPPC (●) and POPC (▲) vesicle solutions, C_s. The Φ_t value estimated from v_i in the DPPC vesicle solution at C_s = 27.7 μM is employed as a standard.

second-order rate constant for excimer formation, C_a is the concentration of M, and k_b is the rate constant for the dissociation of the excimer into M and M*. According to the scheme, I_e/I_m is described by Eq. (1):

$$\frac{I_e}{I_m} = \frac{k_{fe}}{k_{fm}} \tau_e k_a C_a \quad (1)$$

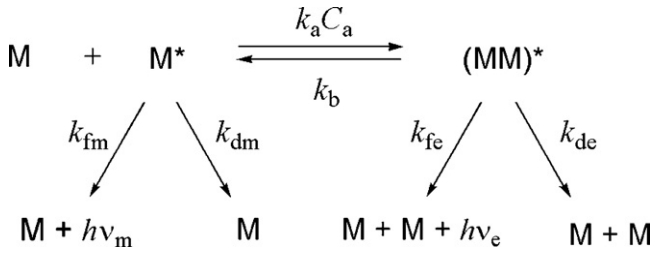

Scheme 2. General scheme for the formation of excimer molecules (MM)*.

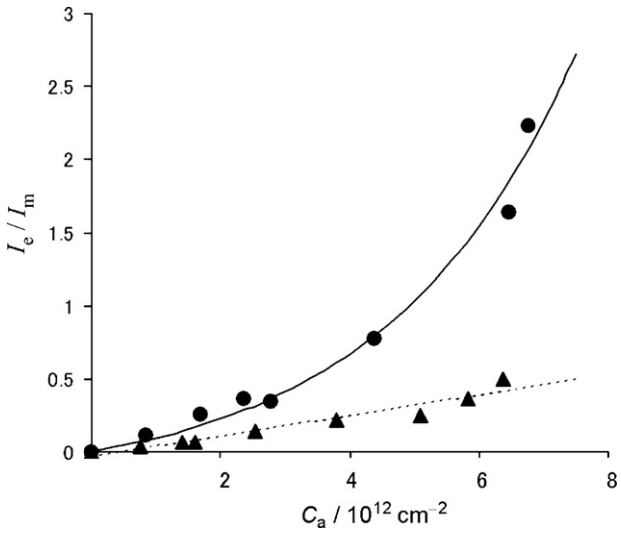

Fig. 4. Plots of the excimer to monomer fluorescence intensity ratio, I_e/I_m, against the $PyCH_2OH$ concentration in the DPPC (●) and POPC (▲) vesicle solutions, C_a, in molecules cm^{-2}. The solid line represents the curve fitted to the experimental data by using the non-linear least-square analysis according to Eq. (3), while the broken line shows a linear relationship between I_e/I_m *vs.* C_a.

In this equation, τ_e is equal to $(k_{de} + k_{fe} + k_b)^{-1}$, which represents the lifetime of the excimer. Galla and Sackmann found that I_e/I_m for pyrene incorporated into DPPC membranes in temperatures above T_m increased linearly with an increase in C_a, indicating that the excimer formation was a diffusion-controlled process, and determined the diffusion coefficient, D_{diff}, for pyrene in DPPC membranes to be 1.40×10^{-7} cm^2 s^{-1} at 50 °C [28]. The parameter D_{diff} is related to the second-order rate constant for the excimer formation, k_a, by Eq. (2):

$$D_{diff} = \frac{\lambda k_a}{4d_c} = \frac{I_e}{I_m} \frac{k_{fm}}{k_{fe}} \frac{\lambda}{4d_c \tau_e} \frac{1}{C_a} \quad (2)$$

where λ and d_c are the length of one diffusional jump and van der Waals diameter of pyrene in the lipid membrane, respectively.

Fig. 4 depicts the plots of the fluorescence intensity ratio, I_e/I_m, against the $PyCH_2OH$ concentration in the DPPC and POPC vesicle solutions prepared for the electron transport experiments. The $PyCH_2OH$ concentration in the vesicle solution, C_s, in μM is converted to the number of $PyCH_2OH$ molecules per unit area of the lipid membrane, C_a, in cm^{-2} by assuming that the vesicles include all lipid molecules employed in the vesicle preparation, and that the area per lipid molecule is 0.6 nm^2. As shown in the figure, a linear relationship is obtained between I_e/I_m and C_a in the liquid-crystalline POPC vesicles, indicating that the excimer formation is a diffusion-controlled process in the POPC vesicles. It seems reasonable to apply the parameters assumed by Galla and Sackmann for pyrene to $PyCH_2OH$ since no significant difference in photophysical properties and molecular size between two pyrenes. Thus, using Eq. (2) and the parameters of k_{fm}/k_{fe} = 0.1 and d_c = λ = 0.8 nm [28], as well as τ_e = 120 ns measured in the vesicle solution of DPPC containing cholesterol (*vide infra*), the diffusion coefficient of $PyCH_2OH$ in the POPC vesicle membranes, D_{diff}, is calculated to be 1.5×10^{-8} cm^2 s^{-1} from the slope of the straight line of Fig. 4 that is equal to $I_e/(I_m C_a) = 7.0 \times 10^{-14}$ cm^2. This D_{diff} value is by a factor of 10 smaller than that of pyrene reported by Galla and Sackmann, but in fair agreement with the phospholipid self-diffusion coefficient and the D_{diff} values of androstane or fatty acids that are anchored at the bilayer–water interface with their hydrophilic groups [22,33].

On the other hand, the plot of I_e/I_m against C_a deviates largely upward from the straight line in the DPPC vesicle that is in the

gel phase, describing that a lateral diffusion model is no longer applied to the excimer formation. As mentioned in the previous section, it is believed that below T_m pyrene molecules embedded in DPPC membranes aggregate to form small clusters, in which the local concentration of pyrene molecules is effectively larger than in the fluid liquid-crystalline membranes [28–30]. To understand a large upward deviation of the I_e/I_m–C_a plot, we apply the Perrin formulation to the excimer formation in the rigid gel membranes [34,35]. According to the Perrin model, in which it is assumed that the excited molecule M* is quenched with unit efficiency by the other molecule M that is located within the quenching sphere, A_q, to form the excimer (MM)*, while M outside of the quenching sphere does not quench M* at all, the rate constant for the excimer formation, $k_a C_a$, in Scheme 2 is replaced by $(k_{dm} + k_{fm})\gamma \exp(A_q C_a)$ where γ is equal to $(k_{de} + k_{fe})/(k_{de} + k_{fe} + k_b)$. Thus, I_e/I_m is described by Eq. (3):

$$\frac{I_e}{I_m} = \frac{\phi_e}{\gamma\phi_m}[\exp(A_q C_a) - 1] \quad (3)$$

where ϕ_m and ϕ_e are fluorescence quantum yields of M* and (MM)*, which are equal to $k_{fm}/(k_{dm} + k_{fm})$ and $k_{fe}/(k_{de} + k_{fe} + k_b)$, respectively. As demonstrated in Fig. 4, it is found that the experimental data are fitted to Eq. (3) with $\phi_e/(\gamma\phi_m) = 0.24$ and $A_q = 3.4 \times 10^{-13}$ cm^2. Therefore, it is presumed that in the DPPC membrane that is in the rigid gel phase, the excited molecule M* is quenched by M located within a 3.3 nm radius of M* with unit efficiency to form the excimer (MM)*. In other words, the area with a radius of 3.3 nm exists in the DPPC membrane, in which the local concentration of M is large enough so that the excitation energy migrates and is trapped by the excimer site located in the area with unit efficiency.

3.2.3. Discussion on the mechanism of transmembrane electron transport in DPPC vesicles

As mentioned in the previous section, photoinduced transmembrane electron transport proceeds in DPPC vesicles that are in the gel phase, indicating that the lateral diffusion of the sensitizers along the membrane surfaces is not indispensable for the reaction. Furthermore, experimental evidence is presented that sensitizer molecules aggregate to form clusters in the DPPC membranes, which could play an important role in transmembrane electron transport. Although the DPPC vesicles used for photoinduced electron transport experiments are prepared by sonication at above T_m, DPPC gel domains form upon lowering the temperature below T_m excluding the sensitizer molecules from the domains, so that the sensitizer molecules concentrate in the fluid phase resulting in formation of an area where the local concentration of the sensitizer is large in the DPPC vesicle membranes [32]. We propose that a pair of the sensitizers in the opposite monolayers of the vesicles exists in this area, where the transmembrane electron exchange between the sensitizers proceeds with high efficiency Φ_E. In the liquid-crystalline POPC vesicles, such a pair of the sensitizers could be formed through lateral diffusion of the sensitizers along the membrane surfaces.

Fig. 3b demonstrates that the total efficiency of photoinduced transmembrane electron transport, Φ_t, decreases largely with an increase in the sensitizer concentration, C_s, in the POPC vesicles. This is a rather curious result because transmembrane electron transfer from $S_i^{-\bullet}$ to S_o would accelerate with an increase in the concentration of S_o resulting in an increase in Φ_E. Although no definite evidence is offered at the present stage, we propose that the decrease of Φ_t with an increase in C_s is due to a significant decrease in the lifetime of reactive intermediates that participate in photoinduced transmembrane electron transport, that is, the sensitizer in its excited state and the sensitizer radical anion. The increase in C_s enhances the interaction of S_i^* with S_i which induces excimer formation, as well as that of $S_i^{-\bullet}$ with S_i which causes the electron exchange between them to increase the chance to encounter the oxidized Asc^- in the inner waterpool. It should be noted, however, that Φ_t is almost unchanged in the C_s range above 10 μM in DPPC vesicles. This observation could be explained in terms of the formation of the sensitizer clusters, which is suggested by the dependence of I_e/I_m on C_s. In the sensitizer clusters, the lifetimes of reactive intermediates would be almost independent of C_s owing to the efficient excited energy migration and electron exchange between sensitizers located close together in the same monolayers.

3.3. Effect of cholesterol on transmembrane electron transport in DPPC vesicles

The addition of cholesterol to phospholipid membranes has a great influence on their properties. Above T_m cholesterol reduces the fluidity of the membranes strongly [23,36]. Galla and Sackmann demonstrated that a cholesterol content of 30 mol% reduced D_{diff} of pyrene embedded in DPPC membranes by a factor of two at 50 °C [28]. On the other hand, they also reported that the dependence of the fluorescence intensity ratio, I_e/I_m, on the pyrene concentration in DPPC membranes with more than 10 mol% cholesterol at 35 °C obeyed the diffusion model, indicating that below T_m cholesterol suppresses the cluster formation of pyrene. Thus, to gain further information about the sensitizer cluster in the electron transport in DPPC vesicle bilayers, the effect of cholesterol on the electron transport efficiency was examined.

A vesicle solution containing cholesterol was prepared in an identical manner to that described in the previous section, except for using DPPC (8 μmol) and cholesterol (4 μmol) instead of DPPC (12 μmol), and irradiated. The results of a typical run (Fig. S2) are summarized in Table 1, indicating that the addition of 33% cholesterol in DPPC vesicles results in a considerable decrease in the rate of $MV^{+\bullet}$ formation, v_i, as well as the maximal concentration of photogenerated $MV^{+\bullet}$, C_{max}. As shown in the table, although the presence of cholesterol reduces C_s slightly, a large decrease in v_i is mainly due to the decrease in a total quantum yield for $MV^{+\bullet}$ formation. Moreover, to gain information about the effect of cholesterol on the interaction of the sensitizer embedded in the membrane with the molecules added in the outer aqueous phase, quenching of the sensitizer fluorescence by MV^{2+} was examined (Fig. S3), the results of which are also shown in Table 1. The table shows that the Stern–Volmer constants, K_{SV}, for the fluorescence quenching are little affected by the addition of cholesterol in the membrane, suggesting that the interaction of the sensitizer embedded in the membrane with the species in the bulk aqueous phase is not disturbed largely by the addition of cholesterol in the membrane. Thus, based on these observations, we propose that the large decrease in the electron transport efficiency by the addition of cholesterol to DPPC membranes is attributed to the destruction of the sensitizer cluster containing a pair of sensitizers in the opposite monolayers. It is thought that the sensitizer mobility in the DPPC membrane is much lower even in the presence of cholesterol compared with that in the POPC membrane at room temperature.

The evidence for the destruction of the sensitizer cluster in the DPPC membrane containing cholesterol was indicated by the fact that the excimer to monomer fluorescence intensity ratio, I_e/I_m, of the sensitizer embedded in the membrane decreased considerably in the presence of cholesterol (Fig. S4). Furthermore, as depicted in Fig. 5, the temperature dependence of I_e/I_m in DPPC vesicles containing cholesterol differs greatly from that in the absence of cholesterol. As the temperature is raised from 10 to 60 °C, in DPPC vesicles containing 33 mol% cholesterol the I_e/I_m value increased monotonously, while in the absence of cholesterol the I_e/I_m value increased slightly at first, but decreased sharply from around 20 °C up to T_m of DPPC vesicles (42 °C), and then increased again above

Table 1
Effect of cholesterol on the electron transport across vesicle bilayers and photophysical properties of $PyCH_2OH$ embedded into the vesicle membrane.

Vesicles	v_i/μM min^{-1}	C_{max}/μM	C_s/μM	Φ_t(rel)[a]	τ_M/ns[b]	τ_E/ns[c]	K_{SV}/M^{-1} [d]
DPPC[e]	0.223	17.8	28.4	1.0	115	89	34.2
DPPC–cholesterol2:1	0.024	5.8	15.5	0.17	185	116	36.0

[a] Relative value of a total quantum yield for $MV^{+\bullet}$ formation evaluated by v_i/I(rel).
[b] Lifetime of the sensitizer monomer fluorescence in the vesicle solutions.
[c] Lifetime of the sensitizer excimer fluorescence in the vesicle solutions.
[d] Stern–Volmer constant for the quenching of the sensitizer monomer fluorescence by MV^{2+} added in the outer aqueous solution.
[e] The results of the electron transport across vesicle bilayers agree with those presented in the previous section within the experimental error.

T_m. The analogous temperature dependence of I_e/I_m was reported in the fluorescence of pyrene or a pyrene-labeled phosphatidylcholine embedded in DPPC vesicle bilayers, which is reasonably interpreted in terms of a lateral redistribution of the fluorescent probe in the temperature range of the phase transition [28,32]. Therefore, this observation provides unambiguous evidence indicating that the sensitizer molecules aggregated into clusters in DPPC vesicles at a temperature below the T_m, and that the addition of cholesterol disrupted the clusters.

Thus, the addition of cholesterol in DPPC vesicle membranes resulted in a considerable decrease in the efficiency of photoinduced transmembrane electron transport. On the basis of the effect of cholesterol on the I_e/I_m values of the sensitizer, we propose that the decrease in the efficiency in the vesicles containing cholesterol is attributed to the destruction of sensitizer clusters, suggesting that the sensitizer clusters play an important role in photoinduced transmembrane electron transport in DPPC vesicles.

3.4. Transmembrane electron transport in DPPC vesicles using various electron donors

To demonstrate the generality of this system, transmembrane electron transport experiments in DPPC vesicles were carried out using electron donors other than AscNa. As electron donors that undergo reversible redox reactions, we examined cysteine (CySH), glutathione (GSH), and iodide ion, and compared their results with those of sacrificial electron donors such as EDTA and TEOA. The method for preparing the vesicle solution employed in the electron transport experiments was identical to that described in the previous section, except for using these electron donors instead of AscNa. The concentration of the sensitizer $PyCH_2OH$ incorporated into the vesicle solution, C_s, was almost independent of the electron donors (23–28 μM). The accumulation of $MV^{+\bullet}$ by the irradiation of the vesicle solution containing various electron donors is displayed in Fig. S5, and the v_i and C_{max} determined by the experiments are summarized in Table 2, showing that this photoinduced electron transport system can work using electron donors other than AscNa, although the efficiency of the electron transport is dependent on the electron donors.

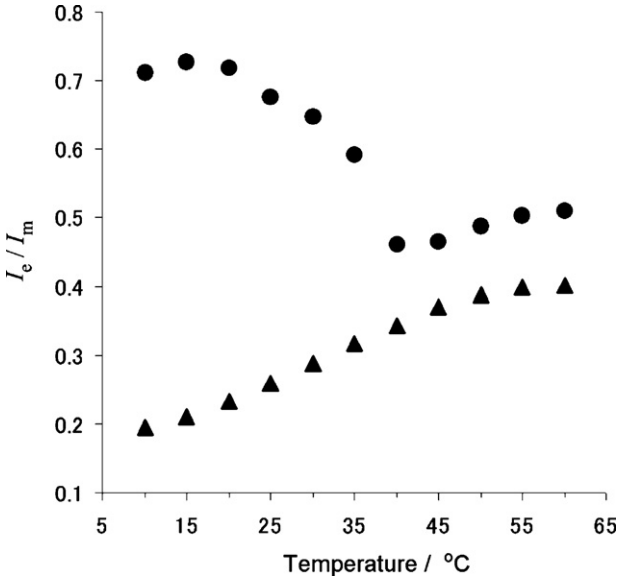

Fig. 5. Temperature dependence of the excimer to monomer fluorescence intensity ratio, I_e/I_m, of $PyCH_2OH$ in the DPPC (●) and DPPC–cholesterol (2:1, ▲) vesicle solutions.

Assuming the mechanism shown in Scheme 1, the properties of electron donors influence the total quantum yield for $MV^{+\bullet}$ formation, Φ_t, by controlling the efficiency for quenching of the sensitizer excited state, Φ_D, as well as the efficiency for $S_i^{-\bullet}$ to transfer an electron to S_o, Φ_E. An increase in the rate constant for quenching of the sensitizer fluorescence by the electron donor, k_q, results in an increase in Φ_D, while an acceleration of the charge recombination of $S_i^{-\bullet}$ with the oxidized electron donor decreases in the lifetime of $S_i^{-\bullet}$ leading to a decrease in Φ_E. To obtain a clue to understanding the effect of the electron donors described above, quenching of the sensitizer fluorescence by the electron donors was examined. Since Stern–Volmer constants, K_{SV}, for quenching of the fluorescence of $PyCH_2OH$ embedded in the vesicle membrane by the electron donors were too small to obtain accurate rate constants for the fluorescence quenching, we carried out quenching studies in an aqueous solution (1.0 M Tris–HCl buffer). The K_{sv} and k_q values determined for each electron donor, as well as its oxidation potential, E_{ox}, are also presented in Table 2. Since the Rehm–Weller equation predicts that the reductive quenching of singlet excited pyrene with these electron donors is exoergic with large negative free-energy changes from −9.6 to −38.7 kcal mol^{-1}, it is reasonable to think that quenching of the sensitizer fluorescence with these donors proceeds by an electron transfer mechanism. As shown in Fig. 6a, no simple relationship is found between the rate of $MV^{+\bullet}$ formation, v_i, and the rate constant for quenching of the sensitizer fluorescence, k_q. This observation seems to imply that quenching of the sensitizer excited state by the electron donor is not a rate-determining step in the transmembrane electron transport reaction, although the possibility that the rate constant for the fluorescence quenching determined in an aqueous solution fails to reflect that for quenching of the fluorescence of the sensitizer embedded in the vesicle membrane cannot be ruled out. However, there is a tendency for the rate of $MV^{+\bullet}$ formation, v_i, to decrease with an increase in the oxidation potential of the electron donors, E_{ox}, except for the sacrificial donors (Fig. 6b). As the free energy change for the charge recombination of the sensitizer radical anion with the oxidized electron donor increases with an increase in E_{ox} of the electron donor, it appears that the acceleration of $MV^{+\bullet}$ formation in electron transport using electron donors having low E_{ox} is attributed to a decrease in the rate of the charge recombination that elongates the lifetime of the sensitizer radical anion. This assumption is supported by the fact that v_i in electron transport using sacrificial donors, in which the charge recombination is suppressed by their irreversible decomposition, is considerably larger than that expected from their E_{ox} (Fig. 6b).

Table 2
Electron transport across DPPC vesicle bilayers sensitized by $PyCH_2OH$ using various electron donors and kinetic parameters for the quenching of $PyCH_2OH$ fluorescence by them in an aqueous solution[a].

Donor[b]	v_i/μM min^{-1}	C_{max}/μM	K_{sv}/M^{-1} [c]	k_q/10^7 M^{-1} s^{-1} [d]	E_{ox}/V[e]
CySH	0.930	36.3	47.6	31.6	−0.43
GSH	0.393	15.1	13.4	8.87	−0.44
AscNa	0.223	17.8	242	160	+0.09
KI	0.048	14.8	159	105	+0.30
EDTA	0.385	34.8	50.3	33.4	+0.79
TEOA	0.230	12.0	74.8	49.6	+0.82

[a] In a Tris–HCl buffer solution (pH 7.6).
[b] CySH: cysteine, EDTA: ethylenediaminetetraacetic acid disodium salt, GSH: glutathione, and TEOA: triethanolamine. The donor concentration in the inner waterpool is 1.0 M, except for EDTA (0.3 M) and GSH (0.5 M).
[c] Stern–Volmer constant for the quenching of $PyCH_2OH$ fluorescence by the donor.
[d] Rate constant for the quenching of $PyCH_2OH$ fluorescence determined by $k_q = K_{sv}/\tau_0$, in which τ_0 is fluorescence lifetime of $PyCH_2OH$ in a Tris–HCl solution (151 ns).
[e] Oxidation potential of the donor (*vs.* SCE) [19,37–40].

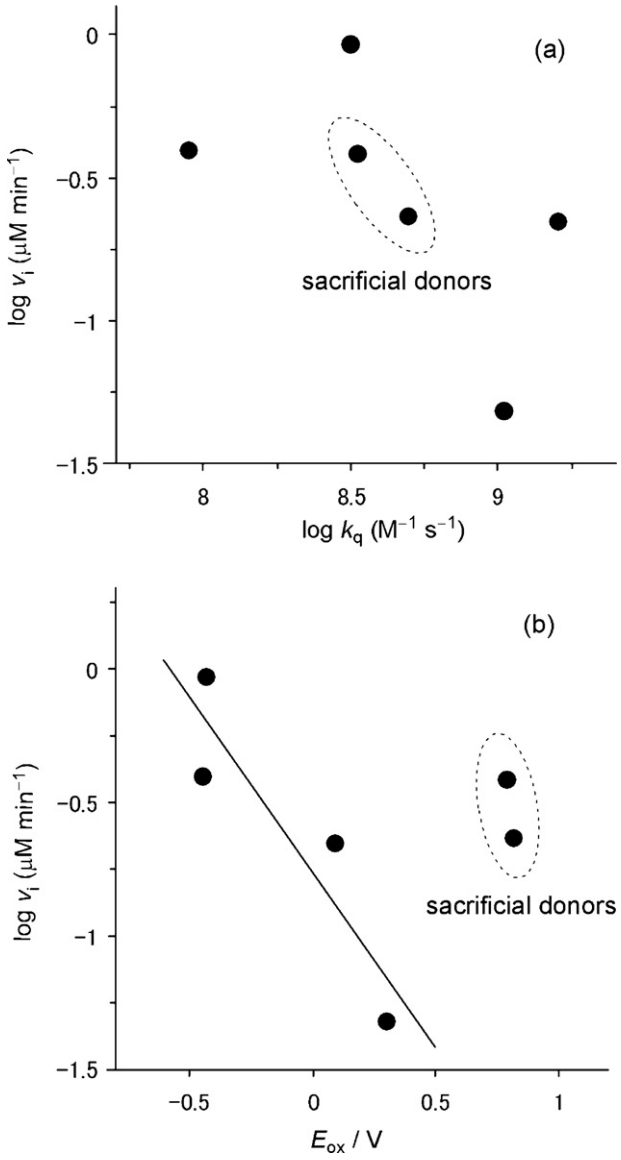

Fig. 6. Relationships of the rate of $MV^{+\bullet}$ formation, v_i, in the photoinduced transmembrane electron transport using various electron donors to (a) the rate constant for quenching of the $PhCH_2OH$ fluorescence by the electron donors, k_q, and (b) the oxidation potential of the electron donors, E_{ox}.

Thus, it is established that various compounds capable of undergoing reversible redox cycles can be used as electron donors entrapped into the inner waterpool of the vesicles in photoinduced transmembrane electron transport. An electron donor having lower oxidation potential, E_{ox}, gave a larger rate of $MV^{+\bullet}$ formation, v_i, which is probably due to the retardation of the recombination of photogenerated charges and not to the acceleration of the quenching of the sensitizer excited state. However, it should be noted that electron donors having low E_{ox} are unfavorable from the viewpoint of light-chemical energy conversion to mimic natural photosynthetic systems. For example, the total electron transfer from CySH to MV^{2+} is almost neutral thermodynamically with a free-energy change of +0.7 kcal mol^{-1}.

3.5. Hydrogen generation based on transmembrane electron transport in DPPC vesicles

Although the electron transport across vesicle bilayers described here is endoergic with a positive free-energy change, ΔG, the resulting $MV^{+\bullet}$ is reactive species that can be easily reoxidized to MV^{2+} by molecular oxygen. In order to achieve the fixation of light energy into the chemical bond energy, this electron transport system should be linked with catalytic reactions, which enable the transformation of materials into their stable reductive form through multielectron processes. Colloidal platinum acts as a catalyst for a dielectronic reduction of water to hydrogen using electrons from $MV^{+\bullet}$ [41–43]. For the last few decades, a photochemical system for hydrogen generation from water has been extensively studied, especially in view of the storage of solar energy using ruthenium(II) complexes as a sensitizer for visible-light absorption. Thus, it is established that hydrogen is evolved from water by visible-light irradiation of aqueous solutions containing the following four components: the $Ru(bpy)_3^{2+}$ complex (bpy = 2,2′-bipyridine), a sacrificial electron donor such as EDTA and TEOA, colloidal platinum as a catalyst, and MV^{2+} that mediates electrons from the sensitizer to the catalyst. As mentioned in the introductory part, however, systems using sacrificial electron donors are of no significance from the viewpoint of storage of light energy, because a considerable amount of chemical energy would be lost by an irreversible decomposition of oxidized sacrificial electron donors. Grätzel and his co-workers presented a photochemical system for hydrogen generation, in which water itself acts as an electron donor using a catalyst composed of Pt and RuO_2 supported by colloidal TiO_2 particles [44,45]. Moreover, extensive studies of hydrogen production from water using a semiconductor photocatalyst with solar energy have been performed, and an efficient nonsacrificial water splitting system operating under visible-light irradiation is reported [46]. However, hydrogen evolution systems mimicking natural photosynthesis with electron donors capable of undergoing reversible redox cycles have not been reported, in

which a design to prevent charge recombination processes would be required.

In principle, a photochemical system for hydrogen evolution using a reversible electron donor would be completed by the addition of both MV^{2+} and colloidal platinum to the aqueous solution of DPPC vesicles containing $PyCH_2OH$ in the vesicle membranes and Asc^- in the inner waterpool. However, besides the limited amount of $MV^{+\bullet}$ generated by photoinduced transmembrane electron transport in vesicles, compared with the considerable amount produced in the solution containing sacrificial electron donors in high concentrations, we should consider the two following problems, both of which were encountered actually in our experiments. First, colloidal platinum is usually prepared by the reduction of H_2PtCl_6 in the presence of surfactants, such as sodium dodecyl sulfate, poly(vinyl alcohol), and poly(*N*-vinyl-2-pyrrolidone) (PVP) [42,47]. Therefore, the surface of the resulting platinum particles is protected by the surfactants that prevent their aggregation. Since surfactants dissolve vesicles, the system of photoinduced transmembrane electron transport would be destroyed by the addition of an aqueous solution containing colloidal platinum to the vesicle solution. Secondly, the ion concentration of the vesicle solution for photoinduced electron transport is considerably high so that an electron donor Asc^- can be encapsulated in high concentrations in the inner waterpool of the vesicles. Since the dispersion of colloidal particles is less stable in the solutions of ions in high concentrations, addition of a solution containing colloidal platinum to the vesicle solution would cause the aggregation of platinum particles to form the precipitates.

For the reasons mentioned above, the concentrations of colloidal platinum and Asc^- entrapped into the inner waterpool of the vesicles are limited to construct the hydrogen evolution system linked with the photoinduced transmembrane electron transport. After examination of various conditions to prepare the vesicle solution containing colloidal platinum, we found that hydrogen was produced by the irradiation of the solution prepared in the following manner; the solution of DPPC vesicles, in which $PyCH_2OH$ (ca. 20 μM) was embedded into the bilayers and AscNa (0.20 M) was entrapped into the inner waterpool, in 0.20 M Tris–HCl buffer (pH 7.5) containing NaCl (0.20 M) was prepared according to a similar method to that described in the previous section. To the solution (3.0 mL), $MVCl_2{\cdot}3H_2O$ and an aqueous solution containing PVP-protected platinum particles (1 mM) were added to give a vesicle solution with MV^{2+} (20 mM) and colloidal platinum (10 μM). In a typical run, after irradiation (366 ± 15 nm) of the solution for 3 h, 24 ppm of hydrogen were detected by the GC analysis of the headspace of the cell (1.5 mL). Simultaneously, the accumulation of 25 μM of $MV^{+\bullet}$ was observed with $v_i = 0.19\ \mu M\ min^{-1}$. Thus, the connection of the system of photoinduced transmembrane electron transport with the system for hydrogen generation by water reduction was accomplished by using MV^{2+} as a mediator.

Based on the results described above, the average rate of hydrogen production is estimated to be 8.2×10^{-12} mol min^{-1}, indicating that only 2.9% of $MV^{+\bullet}$ generated by photoinduced transmembrane electron transport can be used for the reduction of water to hydrogen. Moreover, assuming that the quantum yield for $MV^{+\bullet}$ formation estimated in the $PyCH_2OH$-sensitized transmembrane electron transport in the vesicles of PC from egg yolk can be applied [16,17], the quantum yield for the hydrogen production of this experiment is evaluated to be 0.16%. Although this value is considerably lower compared with the 13% reported in the photochemical hydrogen generation system of EDTA/$Ru(bpy)_3^{2+}$/MV^{2+}/colloidal platinum ([$Ru(bpy)_3^{2+}$] = 0.04 mM, [MV^{2+}] = 2 mM, [EDTA] = 30 mM) [42], we should emphasize the following two points. First, in our system electrons used for the reduction of water are ultimately supplied from not sacrificial electron donors but from a species capable of undergoing a reversible redox cycle. Secondly, the vesicles play an essential role in the hydrogen generation, since the recombination reaction between photogenerated $MV^{+\bullet}$ and oxidized form of Asc^- is suppressed effectively by the hydrophobic vesicle bilayers, and the tiny inner waterpool of the vesicles holds a solution of electron donors in high concentrations. It should be noted that taking into account that the ratio of the total volume of the vesicle inner waterpool to the bulk solution prepared under our conditions is of the order of 0.1%, the Asc^- concentration of 0.2 M entrapped in the inner waterpool is equivalent to that of 0.2 mM in the vesicle solution, which is considerably lower compared with the concentrations of sacrificial donors employed in the photochemical hydrogen generation systems reported.

To date, attempts to enhance the efficiency of electron transfer from $MV^{+\bullet}$ to water through colloidal platinum including the examination of various methods of the catalyst preparation and the experiments at lower pH have been unsuccessful. Recently, it has been demonstrated that certain transition metal complexes serve as efficient catalysts for photochemical hydrogen generation from water [48–51]. The use of these molecular catalysts in place of colloidal platinum enables construction of photochemical hydrogen generation systems free from surfactant molecules. Work is in progress to link our system of photoinduced transmembrane electron transport with hydrogen production facilitated by molecular catalysts.

4. Conclusions

We found that DPPC vesicles can be employed as the reaction field for a photoinduced endoergic electron transport from Asc^- in the inner waterpool to MV^{2+} in the outer aqueous solution. DPPC vesicles are in the gel phase at room temperature, so that the motion of molecules embedded in the vesicle bilayers is totally restricted. These results indicate that the lateral diffusion of sensitizers embedded in the vesicle bilayers does not necessarily participate in photoinduced transmembrane electron transport in vesicles. Although the efficiency of the electron transport is slightly lower than that in the liquid-crystalline POPC vesicles prepared and irradiated under the same conditions, DPPC vesicles are useful as the reaction field for photoinduced transmembrane electron transport, because the experiments using DPPC vesicles afford more reproducible results and are less expensive compared with POPC vesicles.

The observation of intense fluorescence due to the excimer in the solution of DPPC vesicles containing the sensitizer $PyCH_2OH$, as well as the analysis of the dependence of the excimer to the monomer fluorescence intensity ratio, I_e/I_m, on the sensitizer concentration revealed that the sensitizer molecules aggregate to form clusters in DPPC membranes. We propose that the sensitizer clusters play an important role in photoinduced transmembrane electron transport in DPPC vesicles. This assumption is supported by the fact that the destruction of the sensitizer clusters by the addition of cholesterol to DPPC membranes diminished greatly the efficiency of the photoinduced transmembrane electron transport. Moreover, it is revealed that various electron donors that undergo a reversible redox cycle other than Asc^- can be used in photoinduced transmembrane electron transport in DPPC vesicles.

Finally, we connected the photoinduced transmembrane electron transport system with a colloidal platinum catalyst by using MV^{2+} as a mediator to construct a novel system for photochemical hydrogen evolution from water. Although the efficiency of hydrogen production is low at present, this system can work using small amounts of electron donors capable of undergoing a reversible redox reaction instead of a solution of sacrificial electron donors in high concentrations. The results presented here demonstrate

the usefulness of DPPC vesicles in constructing artificial molecular systems for light energy conversion mimicking natural photosynthesis. We are continuing work to reach the final goal, *i.e.*, the construction of artificial systems capable of converting light energy into chemical potential with high efficiency.

Acknowledgements

We thank Professor Fumitaka Mafuné of The University of Tokyo for the cooperation in the preparation of platinum particles. This work supported by a Grant-in-Aid for Scientific Research 20550119 from the Japan Society for the Promotion of Science.

Appendix A. Supplementary data

Supplementary data associated with this article can be found, in the online version, at doi:10.1016/j.jphotochem.2011.04.034.

References

[1] M. Calvin, Acc. Chem. Rec. 11 (1978) 369.
[2] M. Calvin, Energy Res. 3 (1979) 73.
[3] T. Meyer, Acc. Chem. Res. 22 (1989) 163.
[4] D. Gust, T.A. Moore, A.L. Moore, Acc. Chem. Res. 34 (2001) 40.
[5] D. Gust, T.A. Moore, A.L. Moore, in: A.F. Collings, C. Critchley (Eds.), Aritificial Photosynthesis, Wiley, Weinheim, 2005, p. 187.
[6] L. Hammarström, S. Hammes-Schiffer (Eds.), Acc. Chem. Res. 42 (2009) 1859.
[7] J. Whitmarsh, Govindjee, in: G.S. Singhal, G. Renger, S.K. Sopory, K.-D. Irrgang Covindjee (Eds.), Concepts in Photobiology, Kluwer Academic Publishers, Dordrecht, 1999, p. 11.
[8] B. Ke, Photosynthesis, Kluwer Academic Publishers, Dordrecht, 2001.
[9] M. Mangel, Biochim. Biophys. Acta 430 (1976) 459.
[10] W.E. Ford, J.W. Otvos, M. Calvin, Nature 274 (1978) 507.
[11] A.D. Bangham, Prog. Biophys. Mol. Biol. 18 (1968) 29.
[12] D.W. Deamer, P.S. Uster, in: M.J. Ostro (Ed.), Liposomes, Marcel Dekker, New York, 1983, p. 27.
[13] W.E. Ford, J.W. Otvos, M. Calvin, Proc. Natl. Acad. Sci. U.S.A. 76 (1979) 3590.
[14] J.N. Robinson, D. Cole-Hamilton, Chem. Soc. Rev. 20 (1991) 49.
[15] S.V. Lymar, V.N. Parmon, K.I. Zamaraev, Top. Curr. Chem. 159 (1991) 1.
[16] A. Yoshida, A. Harada, T. Mizushima, S. Murata, Chem. Lett. 32 (2003) 68.
[17] T. Mizushima, A. Yoshida, A. Harada, Y. Yoneda, T. Minatani, S. Murata, Org. Biomol. Chem. 4 (2006) 4336.
[18] R. Sasaki, Y. Nako, S. Murata, Tetrahedron 65 (2009) 7364.
[19] D. Njus, P.M. Kelly, Biochim. Biophys. Acta 1144 (1993) 235.
[20] For the calculation of the free-energy change for the total redox reaction, +0.09 V and 0.46 V were employed for the redox potentials of $Asc^{\bullet}/Asc^{-}$ (pH 7.0) [19] and $MV^{2+}/MV^{+\bullet}$ (vs SCE), respectively: S.L. Murov, I. Carmichael, G.L. Hug, Handbook of Photochemistry, 2nd edn., Marcel Dekker, New York, 1993.
[21] J.R. Silvius, in: P.C. Jost, O.H. Griffith (Eds.), Lipid–Protein Interactions, vol. 2, Wiley, Weinheim, 1982, p. 240.
[22] P.F. Devaux, H.M. McConnell, J. Am. Chem. Soc. 94 (1972) 475.
[23] E.-S. Wu, K. Jacobson, D. Papahadjopoulos, Biochemistry 16 (1977) 3936.
[24] E. Steckhan, T. Kuwana, Ber. Bunsen. 78 (1974) 253.
[25] F. Mafuné, J. Kohno, Y. Takeda, T. Kondow, J. Phys. Chem. B 107 (2003) 4218.
[26] N.J. Turro, Modern Molecular Photochemistry, University Science Books, Sausalito, 1991, p. 141.
[27] F.M. Winnik, Chem. Rev. 93 (1993) 587.
[28] H.-J. Galla, E. Sackmann, Biochim. Biophys. Acta 339 (1974) 103.
[29] H.-J. Galla, E. Sackmann, J. Am. Chem. Soc. 97 (1975) 4114.
[30] H.-J. Galla, W. Hartmann, U. Theilen, E. Sackmann, J. Membr. Biol. 48 (1979) 215.
[31] P.J. Somerharju, J.A. Virtanen, K.K. Eklund, P. Vainio, P.K.J. Kinnunen, Biochemistry 24 (1985) 2773.
[32] R.C. Hresko, I.P. Sugár, Y. Barenholz, T.E. Thompson, Biochemistry 25 (1986) 3813.
[33] H. Träuble, E. Sackmann, J. Am. Chem. Soc. 94 (1972) 4499.
[34] N.J. Turro, Modern Molecular Photochemistry, University Science Books, Sausalito, 1991, p. 317.
[35] Y. Waka, K. Hamamoto, N. Mataga, Chem. Phys. Lett. 53 (1978) 242.
[36] D. Marsh, Biochim. Biophys. Acta 363 (1974) 373.
[37] D.A. Keire, E. Strauss, W. Guo, B. Noszál, D.L. Rabenstein, J. Org. Chem. 57 (1992) 123.
[38] A.J. Bard, R. Parsons, J. Jordan, Standard Potential in Aqueous Solution, Marcel Dekker, New York, 1985.
[39] K. Štulīk, F. Vydra, J. Electroanal. Chem. 16 (1968) 385.
[40] R. Ziessel, J. Hawecker, J.-M. Lehn, Helv. Chim. Acta 69 (1986) 1065.
[41] K. Kalyanasundaram, J. Kiwi, M. Grätzel, Helv. Chim. Acta 61 (1978) 2720.
[42] J. Kiwi, M. Grätzel, J. Am. Chem. Soc. 101 (1979) 7214.
[43] M. Kirch, J.-M. Lehn, J.-P. Sauvage, Helv. Chim. Acta 62 (1979) 1345.
[44] E. Borgarello, J. Kiwi, E. Pelizzetti, M. Visca, M. Grätzel, J. Am. Chem. Soc. 103 (1981) 6324.
[45] M. Grätzel, Acc. Chem. Res. 14 (1981) 376.
[46] K. Maeda, M. Higashi, D. Lu, R. Abe, K. Domen, J. Am. Chem. Soc. 132 (2010) 5858.
[47] N. Toshima, Y. Yamada, H. Hirai, Chem. Lett. (1981) 793.
[48] H. Ozawa, M. Haga, K. Sakai, J. Am. Chem. Soc. 128 (2006) 4926.
[49] K. Sakai, H. Ozawa, Coord. Chem. Rev. 251 (2007) 2753.
[50] P. Du, K. Knowles, R. Eisenberg, J. Am. Chem. Soc. 130 (2008) 12576.
[51] S. Fukuzumi, T. Kobayashi, T. Suenobu, Angew. Chem. Int. Ed. 50 (2011) 728.